

Phase Behavior and Structure of Systems Based on Mixtures of *n*-Hentriacontane and Melissic Acid

Lourdes Liliana Serrato-Palacios¹ · Jorge F. Toro-Vazquez¹ ·
Elena Dibildox-Alvarado¹ · Antonio Aragón-Piña² · Maria del Rosario Morales-Armenta¹ ·
Vrani Ibarra-Junquera³ · Jaime David Pérez-Martínez¹

Received: 14 October 2014 / Revised: 13 January 2015 / Accepted: 21 February 2015
© AOCS 2015

Abstract Candelilla wax (CW) organogelation is a promising method for providing structure to solid-like fat-based foods, cosmetics, and drug delivery systems. The main component, *n*-hentriacontane (C31), defines, to a large extent, the thermal properties of CW. CW is a complex mixture of *n*-alkanes, fatty acids, triterpenic alcohols, and fatty alcohols. In this initial examination of the role of CW components on the phase behavior and structure, CW and binary mixtures of C31 and melissic acid (C30) were studied in bulk and in solutions of vegetable oil. Binary mixtures of C31 and C30 presented a predominantly monotectic phase behavior in which the melting temperature of C31 remained constant independently of the mixture composition. Crystal packing of the pure components and mixtures had an orthorhombic subcell, and the microstructures of the mixtures were extremely different from that of the pure components. In solutions with less than 50 % C31, the order–disorder transition observed in bulk C31 was absent. Organogels of C31, C30, or the mixture were softer than those of CW. The increased strength of CW organogels is associated with the relatively small crystal size of this system.

Keywords *n*-Hentriacontane · Melissic acid · Candelilla wax · Organogel

✉ Jaime David Pérez-Martínez
j davidperez@uaslp.mx

¹ Facultad de Ciencias Químicas, Centro de Investigación y Estudios de Posgrado, Universidad Autónoma de San Luis Potosí, Av. Dr. Manuel Nava 6, Zona Universitaria, 78210 San Luis Potosí, SLP, Mexico

² Instituto de Metalurgia, Universidad Autónoma de San Luis Potosí, 78210 San Luis Potosí, Mexico

³ Bioengineering Laboratory, Universidad de Colima, 28400 Coquimatlán, Colima, Mexico

Introduction

Application of vegetable waxes to gel vegetable oil is currently being explored to reduce the intake of fats rich in saturated and *trans* fatty acids [1]. Among the studied waxes, candelilla wax (CW) at concentrations higher than 1 % (w/w) develops vegetable oil organogels with recognized oil retention and textural properties that can produce solid-like water in oil emulsions [2, 3]. Some functional properties can be modulated by the addition of saturated TAGs (i.e., tripalmitin), as well as the application of shearing during the gelation process [4]. According to previous reports, the main components of CW are *n*-alkanes, with *n*-hentriacontane (C31; 35.5 %) as the major constituent, triterpenic alcohols (24.8 %), fatty acids with an even number of carbons (16.6 %, of which 7.8 % is melissic acid), fatty alcohols (3.61 %), and C39 to C64 esters (5.83 %) [3]. Despite the large number of components, CW phase behavior is attributed almost exclusively to the C31 phase transitions because both CW and C31 have an orthorhombic subcell packing at room temperature [4, 5]. Within this context, it has been hypothesized that some CW components are incorporated into the C31 crystal lattice and that others melt at temperatures close to the C31 melting point [3, 4]. Nonetheless, the type of solid phase structure (i.e., solid solution, compound, solid dispersion) of CW remains unknown. This information is fundamental to understand and tailor the functionality (e.g., melting profile, organogelling capacity, and rheological properties) of this natural wax.

The phase behavior of long-chain *n*-alkanes and fatty acids has been extensively studied, but mixtures of these compounds are largely unexplored. To the best of our knowledge only Benziane et al. [6] have studied this type of mixture and observed a eutectic behavior of

binary mixtures of *n*-eicosane (C20; m.p. = 35.80 °C)/lauric acid (C12; m.p. = 43.00 °C), *n*-octacosane (C28; m.p. = 60.10 °C)/palmitic acid (C16; m.p. = 60.60 °C), and *n*-tetracosane (C24; m.p. = 51.3 °C)/stearic acid (C18; m.p. = 69.65 °C) with eutectic mixtures (i.e., mixture with the lowest melting point) of $x_{C20} = 0.55$, $x_{C28} = 0.4$, and $x_{C24} = 0.85$, respectively. That is, the solid phases of these *n*-alkane/fatty acid mixtures were dispersions of one crystalline entity rich in *n*-alkanes and one rich in fatty acids. It was also evident that all components displayed melting temperature depression, but a differential behavior was observed as a function of the melting temperatures of pure components in the binary mixture. A relevant aspect that has also been overlooked is the mixing impact of the system compositions on crystal microstructure. It is known that mixtures of stearic alcohol and stearic acid produce smaller crystals than pure compounds [7, 8]. Thus, modulation of the crystal habit could be used to tailor rheological properties and/or oil binding capacity of wax-based organogels. The aim of this investigation was to develop a phase diagram and study the microstructure of the binary system *n*-hentriacontane (C31)/triacontanoic acid (C30; melissic acid) in bulk and in high oleic safflower oil solutions to model the candelilla wax crystal phase.

Materials and Methods

Refined CW was obtained from Multiceras (Monterrey, Mexico), and C31 ($\geq 99\%$ purity; Sigma) and C30 ($\geq 98\%$ purity; Fluka) were used as delivered. Mixtures were prepared in molar fraction ratios. Compounds were weighed and mixed in the sample container, heated to 10 °C above the highest melting compound for 20 min, and mechanically stirred to obtain a compositionally homogeneous system. To evaluate the solvent effect, the CW, pure components, and selected mixtures were added (4–90 % wt/wt) to high oleic safflower oil (HOSFO), heated to complete melting under constant stirring for 15 min, cooled to room temperature, and immediately used.

Differential Scanning Calorimetry

Crystallization and melting profiles of the pure components, mixtures, and solutions were determined in a DSC (model 2920; TA Instruments New Castle, DE, USA) equipped with a refrigerated cooling unit. Prior to analysis, the DSC was calibrated with indium (melting temperature of 156.6 °C and heat of melting of 28.45 J/g). An empty aluminum pan was used as a reference. The DSC cell was purged with nitrogen (99.99 % purity) flow of 25 mL/min. The sample (2.5–3 mg) sealed in the pan was heated at 15 °C above the melting point of the compound in the

system with the highest melting temperature; after 20 min at this temperature the sample was cooled (5 °C/min) until achieving 30 °C for 1 min, then the system was heated (5 °C/min) to 15 °C above the system melting temperature. Using the first derivative of the heat flow, we calculated the melting enthalpy, temperature at the onset and maximum of the endotherms with the equipment software (Universal Analysis 2000 Ver. 4.2E; TA Instruments-Waters LLC). For each system, at least two independent determinations were performed.

Polarized Light Microscopy

Microphotographs were obtained using a polarized light microscope (BX50; Olympus Optical Co, Ltd., Tokyo, Japan) equipped with a digital color video camera (KPD50; Hitachi Digital, Tokyo, Japan), temperature-controlled stage LTS 330, and temperature control station LTS350 Linkam (Scientific Instruments, Waterfield, UK). Samples of the systems (3 mg) were placed over a glass slide and heated for 20 min at the melting temperature determined using DSC, and a coverslip was placed on the molten sample. Microphotographs of the systems were obtained after 24 h of storage at 25 °C using the Linksys software version 1.3.1. (Linkam Scientific Instruments, Waterfield, UK).

Wide-angle X-ray Diffraction

Wide-angle X-ray (WAX) diffraction patterns of pure components and solutions were performed in an X-ray diffractometer (Panalytical, X'Pert Pro; Almelo, the Netherlands) with CuK α R X-rays ($\lambda = 1.54$ Å) operating at 35 kV and 30 mA and a 0.5° divergence slit, 1° scatter slit, and 5.5 mm receiving slit. Bulk materials and organogels were developed and stored using the same thermal conditions as for microscopy. Prior to analysis, bulk samples were finely grated, and organogels were gently stirred to avoid preferential orientation of the crystallites. Diffraction patterns were obtained by scanning the samples from 16° to 35° using a step of 0.02° and a scan rate of 0.039789°/min. The X'Pert Data Collector version 2.0 was used to analyze the diffraction patterns.

Hardness Measurements

Glass containers (2.4 cm \times 19 mm I.D.) were filled with 3.0 g of the corresponding solution (90 °C) and stored at 25 °C for 24 h. We determined the penetration work ($g_f \cdot mm$) of the corresponding gels using a texture analyzer (LRFA 1500; Brookfield, USA) fitted with a plastic cylindrical probe (35 mm length \times 12.7 mm diameter; TA10; Brookfield, USA). The measurements were obtained at room temperature (≈ 25 °C) in compression mode,

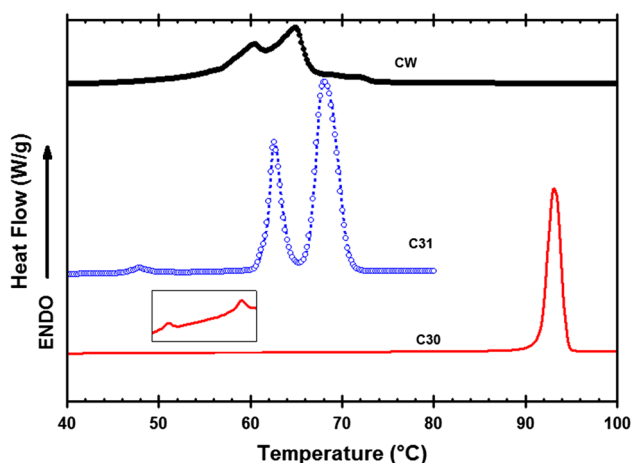


Fig. 1 Heating thermograms for CW candelilla wax, C31 *n*-hentriacontane, and C30 melissic acid. The insert is the enlarged section of the heating thermogram between 40 and 60 °C for C30

penetrating 4 mm into the sample at 1 mm/s and returning to initial position at the same speed. Four independent measurements were obtained for each treatment condition.

Results and Discussion

DSC thermograms and X-ray diffraction patterns of CW and pure C31 and C30 are shown in Figs. 1 and 2. The thermal behavior and X-ray diffraction pattern of CW presented here will be compared with those of the pure compounds and mixtures below. These data were reviewed in the “Introduction” of this manuscript and have been extensively discussed elsewhere [3, 5, 9].

The heating thermogram of C31 showed three endothermic transitions (Fig. 1), and the corresponding transitions were also observed in the cooling thermograms (not shown). In accordance with the thermodynamic data of Briard et al. [10], the C31 endotherms were associated with the following phase transitions: orthorhombic→monoclinic (γ transition; $T_{\gamma, C31} = 47.89 \pm 0.29$ °C), monoclinic→rotor phase (o–d transition; $T_{o-d, C31} = 62.16 \pm 0.05$ °C), and rotor phase→liquid (melting transition; $T_{m, C31} = 67.56 \pm 0.11$ °C). These transition temperatures, as well the total change in enthalpy from the onset of the o–d transition to the end of melting ($\Delta H_{C31} = 244.56$ J/g), were in agreement with that reported by Briard et al. [10]; however, this was not the case with the temperature and enthalpy of the γ transition, which were lower in the present study. The higher reported temperature and enthalpy values [10] were associated with crystal lattice annealing that was performed during heating at 0.5 °C/min. The orthorhombic phase of C31 at room temperature was confirmed using powder XRD (Fig. 2). The C31 diffraction

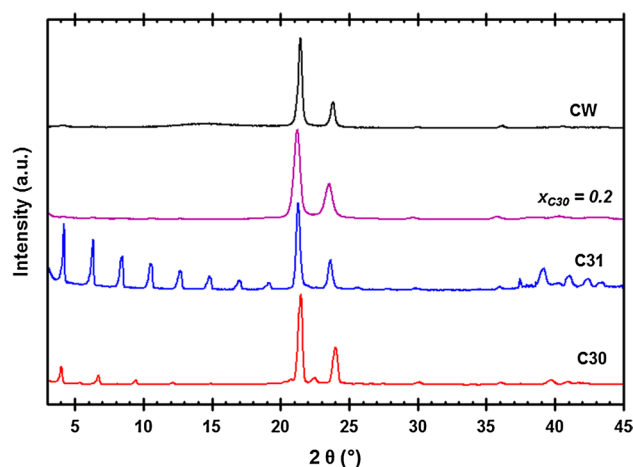


Fig. 2 X-ray powder diffractograms for CW candelilla wax, C31 *n*-hentriacontane, C30 melissic acid, and the C31/C30 mixture with a 0.2 mol fraction of C30 ($x_{30} = 0.2$)

pattern in the wide angle region ($2\theta > 20^\circ$) showed two high intensity peaks at 21.3° and 23.6° and four low intensity peaks in the 38–44° region which are distinctive of long-chain odd *n*-alkanes with an orthorhombic lateral packing [11, 12]. Unit cells of odd *n*-alkanes have similar dimensions in short spacings, but long spacings (001) change proportionally to the length of the molecules and the tilting of chains. In polymorphs with an orthorhombic lateral packing, long spacings depend on the number of carbons because the long axis of the molecule lies perpendicular to the lamellar layer. C31 showed harmonics of diffraction peak (001) because $2\theta = 6.2^\circ$. On the basis of the harmonics we calculated the *d* spacing of 001 = 41.92 Å; this value was in agreement with that predicted using the equation developed for homologous series of *n*-alkanes by Nyburg and Potworowski [13].

C30 heating resulted in one main primary endotherm at $T_{m, C30} = 93.14$ °C ($\Delta H_{m1} = 248.90$ J/g) and two small endotherms (<0.5 J/g) at 59.98 and 51.89 °C (Fig. 1). The corresponding transitions were also observed in the cooling thermogram (not shown). In the X-ray diffractogram (Fig. 2), this compound showed two intense peaks in the wide angle region corresponding to the orthorhombic lateral packing. Crystallographic modifications of even *n*-alkanoic acids have orthorhombic (E_o , B_o), triclinic (*A* form), or monoclinic (B_m and *C* forms) unit cells, but in all cases the lateral packing (i.e., subcell) is orthorhombic. The detailed unit cell is determined for materials crystallized from solution using single crystal X-ray diffraction. In the X-ray powder diffraction patterns of substances with one long unit cell parameter, peak overlapping occurs, and, therefore, it is impossible to determine the unit cell type from this information. However, the main peaks in the 2θ region from 20° to 25° in this work were similar to those

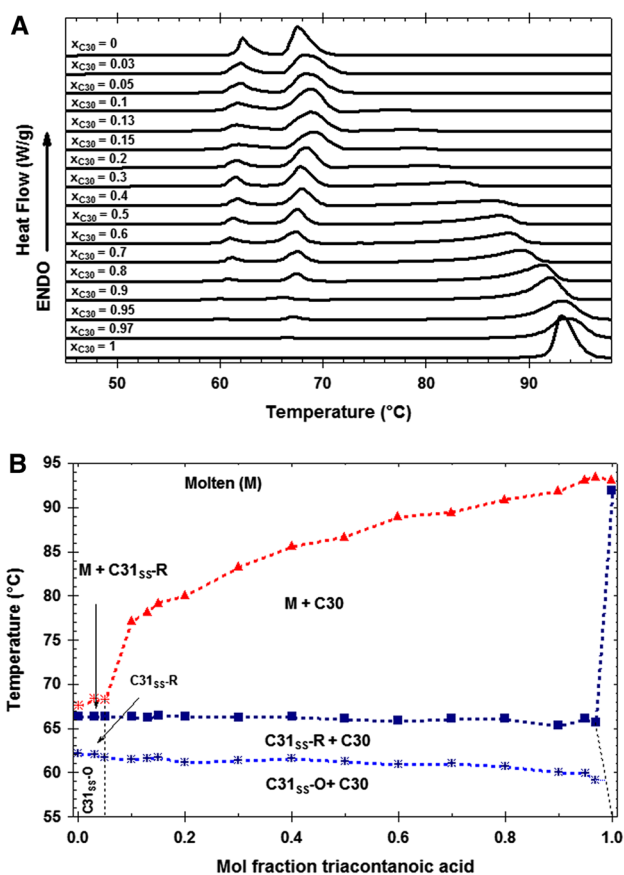


Fig. 3 **a** Melting endotherms for binary mixtures of *n*-hentriacontane (C31) and melissic acid (C30). Binary mixtures are identified by the C30 mol fraction (x_{C30}). **b** Phase diagram for the C31/C30 mixture. Filled triangles represent the highest melting peak in the mixture ($T_{m,C31}$ or $T_{m,C30}$); filled squares represent the onset temperature of the melting peak ($T_{o,C31}$ or $T_{o,C30}$); and asterisks represent the temperature of the o–d transition of C31 crystals ($T_{o-d,C31}$). *M* molten mixture, *C30* crystal rich in C30, *C31_{SS}-R* crystal rich in C31 in rotator phase, *C31_{SS}-O* orthorhombic phase

reported by Garti et al. [14] for stearic acid in the C polymorphic form.

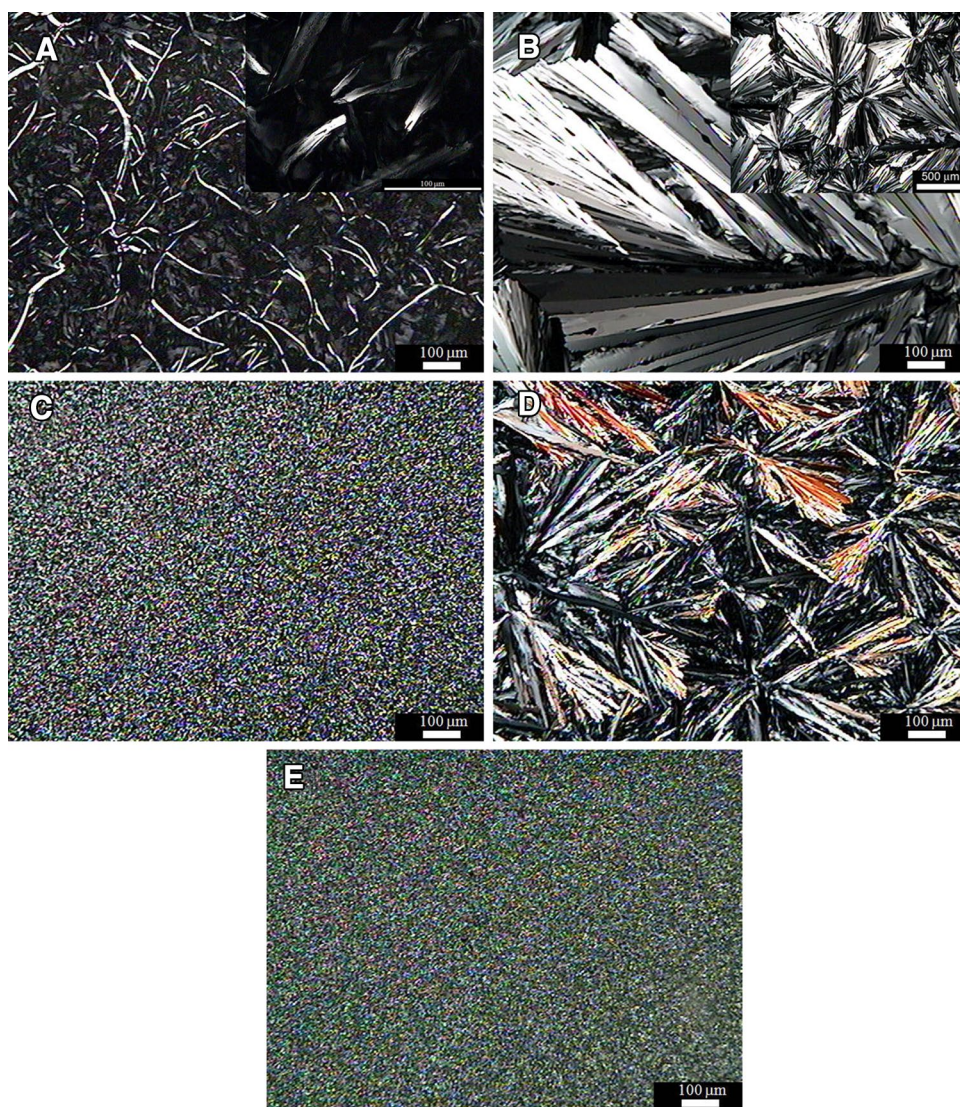
Melting thermograms of binary mixtures of C31 and C30 are shown in Fig. 3a. In these mixtures, the o–d and melting transitions of C31 occur at $T_{o-d,C31} = 61.15 \pm 0.8$ °C and $T_{m,C31} = 66.13 \pm 0.29$ °C independent of the composition. The γ transition, observed in pure C31, was not detected. Conversely, crystalline phases associated with C30 changed with the system composition. Thus, mixtures with a mole fraction of C30 (x_{C30}) from 0.8 to 0.9 displayed a single peak in the melting endotherm, similar to that observed in pure C30. However, mixtures with x_{C30} from 0.2 to 0.7 displayed an additional small endothermic peak at approximately 73.5 °C. This was also observed in the cooling thermogram (data not shown), and it may be associated with the crystallization of an unstable polymorphic modification

of C30 (e.g., polymorphic form E). At lower concentrations, two relevant thermal events were observed: (1) a significant recrystallization exotherm (≈ 72 °C) in mixtures with $x_{C30} = 0.2$ and 0.1 and (2) mixtures with $x_{C30} \leq 0.05$ had no detectable C30 melting endotherm. From these thermal events, it was evident that mixtures with $x_{C30} < 0.05$ developed a solid solution rich in C31 (C31_{SS}). Considering the absence of the γ transition due to co-crystallization with minor amounts of impurities [15] and the recrystallization of C30 at temperatures over the $T_{m,C31}$ in mixtures with $x_{C30} = 0.2$ and 0.1, we conclude that the crystal lattice of C31 crystals contained less than 5 % of C30, independent of the mixture composition.

Regions of the C31/C30 phase diagram were delimited by three temperature lines (Fig. 3b): the liquidus line, represented as dots with filled triangles and corresponding to the temperature at the highest melting peak in the mixture ($T_{m,C31}$ or $T_{m,C30}$); the solidus line, represented as dots with filled squares and corresponding to the onset temperature of the melting peak ($T_{o,C31}$ or $T_{o,C30}$); and the solid transition line represented by dots with asterisks and corresponding to the temperature of the o–d transition of C31 crystals ($T_{o-d,C31}$). Thus, at temperatures above the liquidus line, the mixture was completely molten. Between the liquidus and solidus lines, a molten mixture and a solid crystal phase co-existed. The solid phase was either a solid solution rich in C31 (C31_{SS}) in a mixture with $x_{C30} \leq 0.05$ or C30 crystals if the mixture had $x_{C30} \geq 0.1$. Thus, mixtures found at temperatures below the solidus line and above the solid transition line developed fully crystallized systems: a monophasic system of C31_{SS} in rotator phase in mixtures with $x_{C30} \leq 0.05$ or a biphasic system with C31_{SS} in rotator phase and C30 crystals at $x_{C30} \geq 0.1$. Below the solid transition line, the C31_{SS} changed from a rotator to an orthorhombic modification. The predominantly monotectic behavior of this mixture was consistent with the behavior shown by binary mixtures of triacylglycerols [16] and mixtures of diacylglycerols [17] in which the difference between the melting temperatures of the system components (ΔT_M) was close to or above 20 °C. On the other hand, mixtures of *n*-tetracosane/stearic acid ($\Delta T_M \approx 19$ °C) had a eutectic phase diagram and solid solutions (only one melting endotherm was evident) at mole fractions below 0.15 stearic acid [6]. From this analysis, *n*-alkanes in CW not only co-crystallize small fractions of long-chain fatty acids but also cause an important decrease in the melting temperature (>20 °C) of the fatty acid fraction.

As observed in Fig. 4, the microstructures of C31 and C30 were greatly modified by mixing. C31 grew in large plates and flat fibers (Fig. 4a) and developed a continuous network with the flat fiber branches (e.g., permanent junction zones in organogels). Pure C30 had a spherulitic shape characterized by radial growth from a nucleation

Fig. 4 Polarized light micrographs of bulk materials crystallized at 25 °C. **a** *n*-Hentriacontane, **b** melissic acid, **c** *n*-hentriacontane/melissic acid mixture with a 0.2 mol fraction of melissic acid ($x_{30} = 0.2$), **d** *n*-hentriacontane/melissic acid mixture with a 0.8 mol fraction of melissic acid ($x_{30} = 0.8$), and **e** candelilla wax. The *inserts* in **a** and **b** show the microstructural features of the same sample at higher and lower magnification, respectively



point (Fig. 4b). This type of spherulitic growth has been associated with systems in which the viscosity of the liquid phase is critically high [18]. According to the correlation of van Velzen et al. [19], C30 had a viscosity at least ten times higher than C31 at the same temperature. Thus, addition of C31 to C30 reduced the molten phase viscosity, thus increasing the nucleation rate and producing a higher number of smaller C30 crystals. As C30 crystallized before C31, the C30 crystals acted as nucleation sites and caused a significant reduction in the C31 crystal size (Fig. 4c, b). Similar effects on crystal size resulting from mixing have been observed in other organogelator mixtures [7, 8], and this effect may be the main cause of the characteristic microcrystals of refined CW (Fig. 4e).

Solutions with concentrations higher than 50 % C31 had one endotherm with three peaks associated with the phase transitions observed in pure C31 (Fig. 5a). The γ and o-d transition temperatures remained constant at

$T_{\gamma, C31} = 47.62 \pm 0.73$ °C and $T_{o-d, C31} = 62.45 \pm 0.11$ °C, respectively, but the melting temperature ($T_{m, C31}$) decreased from 66.73 ± 0.07 °C in the 90 % C31 solution to 64.23 ± 0.23 °C in the 60 % C31 solution. Conversely, solutions with ≤ 50 % C31 only exhibited the melting transition of C31 crystals. Notably, at concentrations (1–4 % w/w) typically used to organogel vegetable oils, the o-d transition of C31 is absent. Melting curves of C30 solutions (Fig. 5b) had a single endothermic peak at all studied concentrations, which decreased from 92.54 ± 0.02 °C to 65.13 ± 1.11 °C in 90 and 4 % C30 solutions, respectively.

The binary mixture of C31/C30 with $x_{C30} = 0.2$ was used as a model of refined CW in HOSFO solutions; these data were compared with solutions of the pure components to elucidate the phase behavior. Melting thermograms of these solutions (Fig. 5c) showed a varying number of endothermic peaks depending on the percentage of the C31/C30 mixture. The 90 % C31/C30 solution showed

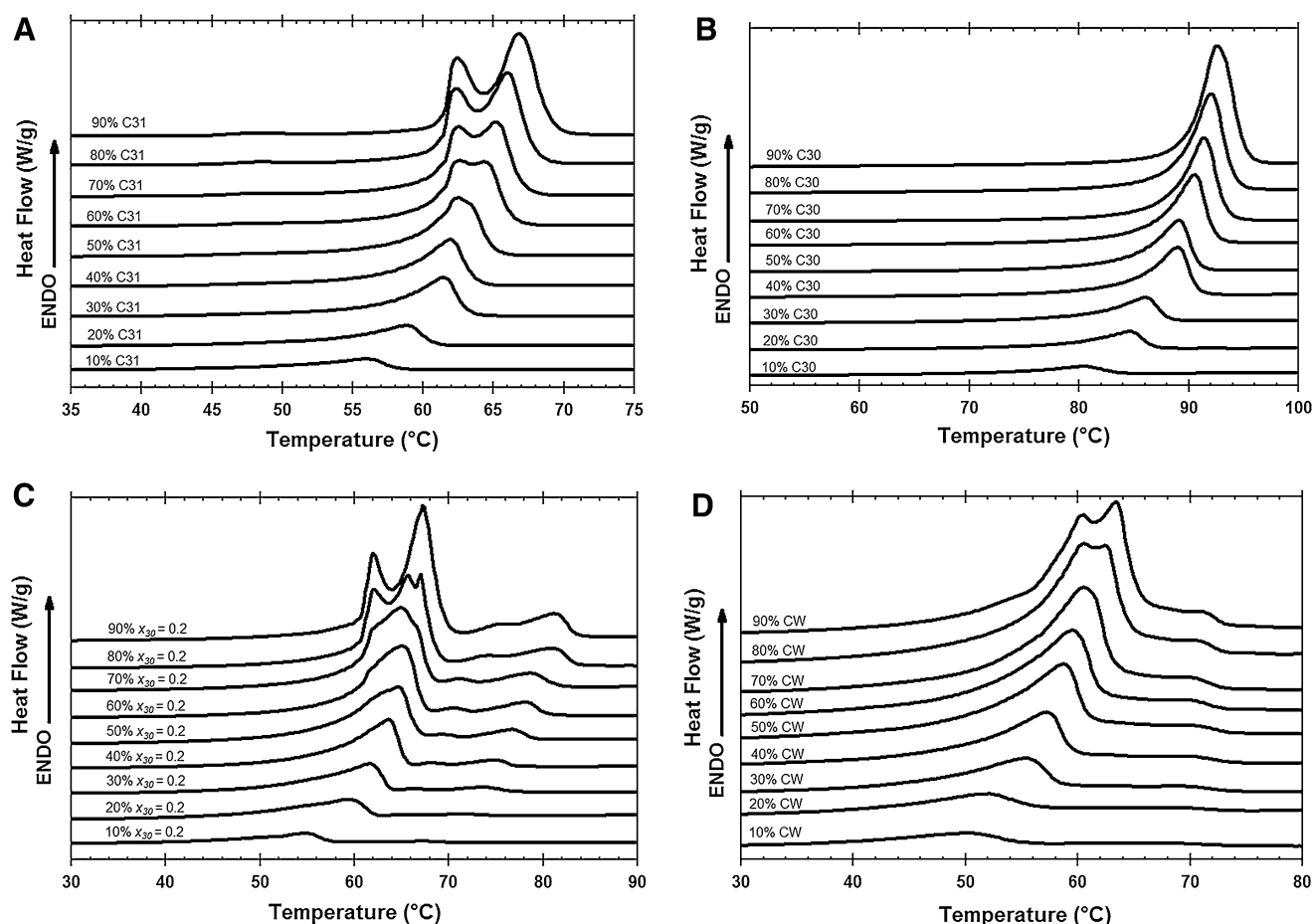


Fig. 5 Melting endotherms for solutions of **a** *n*-hentriacontane (C31), **b** melissic acid (C30), **c** *n*-hentriacontane/melissic acid mixture with $x_{C30} = 0.2$, and **d** candelilla wax (CW) in high oleic safflower

oil (HOSFO). Thermograms are identified by their organogelator-HOSFO proportion (% wt/wt)

an endotherm with four peaks, revealing three important features: (1) the absence of the γ transition of C31 crystals as a result of the incorporation of C30 into their crystal lattice, (2) the lower temperatures of o-d and melting transitions of C31, and (3) the higher melting temperature of the two crystalline species rich in C30 (Fig. 5c). Solutions with a 70–80 % mixture had an additional endothermic transition (≈ 67.3 °C) at a temperature very close to the melting peak temperature of C31 in the undiluted C31/C30 mixture. These transitions were assumed to be the melting of another fraction of C31 crystals because it did not affect the transitions associated with C30. In dilute solutions (≤ 60 % of C31/C30), the melting and o-d transitions of C31 increasingly overlapped, reaching a point (40 % of C31/C30) in which only the melting transition was detected; this was similar to solutions with ≤ 50 % of pure C31 (Fig. 5a). In contrast to C31 melting, the dilution effects in C30 were limited the temperature of the endothermic peaks (Fig. 5c).

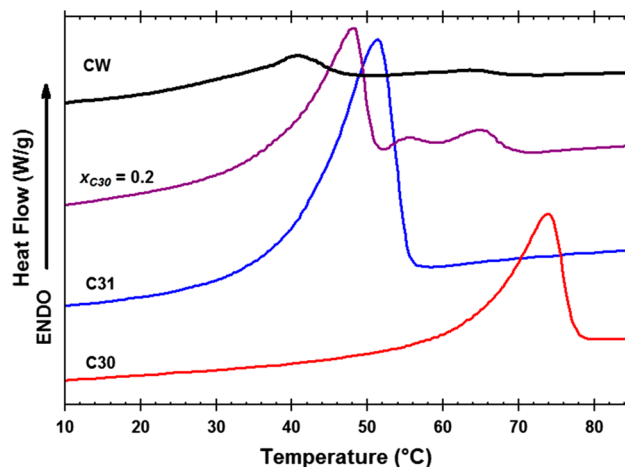


Fig. 6 Melting endotherms for solutions with 4 % (wt/wt) candelilla wax (CW), *n*-hentriacontane/melissic acid mixture with a 0.2 mol fraction of melissic acid ($x_{C30} = 0.2$), C31 *n*-hentriacontane, or C30 melissic acid

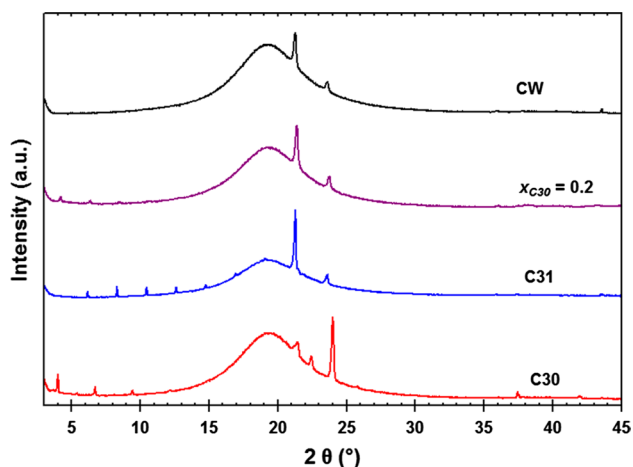
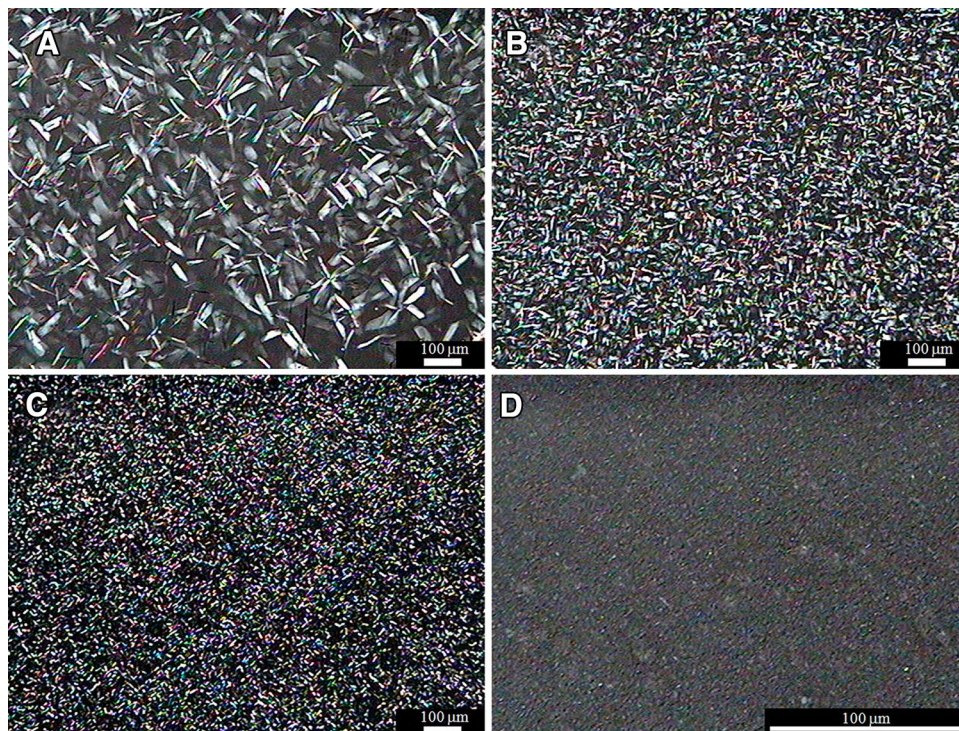


Fig. 7 X-ray powder diffractograms for solutions with 4 % (wt/wt) of candelilla wax (CW), *n*-hentriacontane/melissic acid mixture with 0.2 mol fraction of melissic acid ($x_{C30} = 0.2$), C31 *n*-hentriacontane, or C30 melissic acid

Melting behavior of the model mixture and CW solutions under a wide range of concentrations showed a similar pattern. Thus, CW solutions (Fig. 5d) had a variable number of overlapping endotherms that were reduced in number by CW dilution. Solutions with 80–90 % CW had an endotherm similar to pure CW. Peak temperatures for the 90 % CW solution were $T_{CW1} = 60.33 \pm 0.11$ °C, $T_{CW2} = 63.33 \pm 0.18$ °C, $T_{CW3} = 67.87 \pm 0.25$ °C, $T_{CW4} = 71.33 \pm 0.15$ °C, and $T_{CW5} = 74.93 \pm 0.27$ °C,

with a total enthalpy of $\Delta H_{MT} = 128.45 \pm 3.1$ J/g. On the basis of the endotherm shape, the T_{CW1} and T_{CW2} peaks were associated with the o–d and melting transitions of the *n*-alkanes (e.g., C31), whereas the other peaks corresponded to the melting of other groups of CW components (e.g., aliphatic acids). Dilute CW solutions (≤ 70 % CW) had no peaks corresponding to the o–d transition of *n*-alkanes, which was similar to the ≤ 60 % model mixture solutions. Highly diluted solutions with ≤ 10 % CW exhibited two peaks that were assigned to the melting of *n*-alkanes and to a wide variety of other aliphatic compounds (e.g., acids, alcohols). Solutions containing 4 % CW, pure compounds, or the C31/C0 mixture in HOSFO were used to develop organogels at 25 °C. The organogel crystal phase had melting peaks between 40 and 74 °C (Fig. 6) with an orthorhombic subcell packing [11, 14]. In the wide-angle region, the main diffraction peaks in the organogels were observed in the bulk materials (Figs. 2, 7). Conversely, the relative intensity of the diffraction peaks in the short-angle region of organogels was weak compared to the bulk materials; this resulted from the significant size reduction of the crystal domain in such solutions. The solid fat content (SFC) of these organogels was estimated using DSC as the perceptual ratio between the melting enthalpy of the organogel and the corresponding bulk material. SFC estimates were 6.97, 4.33, 5.65, and 3.59 % for C31, C30, C31/C30 mixture with $x_{C30} = 0.2$, and CW, respectively. Evidently, these values overestimated the actual SFC; therefore, they were used solely for comparative purposes. CW

Fig. 8 Polarized light micrographs of solutions with 4 % (wt/wt) of **a** *n*-hentriacontane, **b** melissic acid, **c** *n*-hentriacontane/melissic acid mixture with a 0.2 mol fraction of melissic acid ($x_{C30} = 0.2$), and **d** candelilla wax



organogel (7.75 ± 0.77 mJ) was at least two times harder than C31 (3.38 ± 0.39 mJ) and C30 (2.77 ± 0.16 mJ) organogels. The C31/C30 mixture (1.63 ± 0.11 mJ) had the lowest resistance to penetration. In plastic fats from TAGS, texture is primarily associated with SFC, crystal size, and the crystal network packing (e.g., fractal dimension). However, in polycrystalline organogels reported here, the permanent junction (crystal branches) plays a major role. This was particularly evident in organogels with similar crystal packing (e.g., 4 % C31/C30 and 4 % C30; Fig. 8), in which the system with higher SFC and smaller crystals (e.g., 4 % C31/C30; Fig. 8) was less hard. Within this context, mixing C31 with C30 modified the nucleation and crystal growth process of C31 and substantially reduced the number of permanent junction zones in the organogel. Accordingly, the elastic properties of CW were primarily associated with its characteristic small size.

Conclusions

Binary mixtures of C31 and C30 presented a predominantly monotectic phase behavior and showed an important decline in the C30 melting temperature and constant temperature transitions (i.e., o–d, melting) for C31 in mixtures. Below the solidus line, a solid dispersion of one phase rich in C31 and another rich in C30 were obtained. The subcell of pure components and their mixtures were orthorhombic. In spite of this, microstructures of C31 and C30 in mixtures were different from that shown in pure systems; these differences were primarily associated with the heterogeneous crystallization and the viscosity differential between pure systems and mixtures. In vegetable oil solutions with less than 50 % C31, only the C31 melting transition was present and the o–d transition observed in C31 in bulk was absent. Organogels of C31, C30, or the mixture were softer than that of CW, and the higher strength of CW organogels was associated with the relatively small crystal size of this system.

Acknowledgments This research was supported by the National Council for Science and Technology of Mexico (CONACYT) through grant number 135133.

References

- Marangoni AG, Garti N (2011) An overview of the past, present, and future of organogels. In: Marangoni AG, Garti N (eds) *Edible oleogels: structure and health implications*. AOCS, Urbana, pp 1–18
- Blake AI, Co ED, Marangoni AG (2014) Structure and physical properties of plant wax crystal networks and their relationship to oil binding capacity. *J Am Oil Chem Soc* 91:885–903. doi:10.1007/s11746-014-2435-0
- Toro-Vazquez JF, Mauricio-Perez R, Gonzalez-Chavez MM, Sanchez-Becerril M, Ornelas-Paz JJ, Perez-Martinez JD (2013) Physical properties of organogels and water in oil emulsions structured by mixtures of candelilla wax and monoglycerides. *Food Res Int* 54:1360–1368. doi:10.1016/j.foodres.2013.09.046
- Chopin-Doroteo M, Morales-Rueda JA, Dibildox-Alvarado E, Charo-Alonso MA, de la Pena-Gil A, Toro-Vazquez JF (2011) The effect of shearing in the thermo-mechanical properties of candelilla wax and candelilla wax-tripalmitin organogels. *Food Biophys* 6:359–376. doi:10.1007/s11483-011-9212-5
- Toro-Vazquez JF, Morales-Rueda JA, Dibildox-Alvarado E, Charo-Alonso M, Alonzo-Macias M, Gonzalez-Chavez MM (2007) Thermal and textural properties of organogels developed by candelilla wax in safflower oil. *J Am Oil Chem Soc* 84:989–1000. doi:10.1007/s11746-007-1139-0
- Benziane M, Khimeche K, Dahmani A, Nezar S, Djalal T (2012) Experimental determination and prediction of (solid+liquid) phase equilibria for binary mixtures of heavy alkanes and fatty acids. *Mol Phys* 110:1383–1389. doi:10.1080/00268976.2011.650229
- Schaink HM, van Malssen KF, Morgado-Alves S, Kalnin D, van der Linden E (2007) Crystal network for edible oil organogels: possibilities and limitations of the fatty acid and fatty alcohol systems. *Food Res Int* 40:1185–1193. doi:10.1016/j.foodres.2007.06.013
- Gandolfo FG, Bot A, Floter E (2004) Structuring of edible oils by long-chain FA, fatty alcohols, and their mixtures. *J Am Oil Chem Soc* 81:1–6. doi:10.1007/s11746-004-0851-5
- Dassanayake LSK, Kodali DR, Ueno S, Sato K (2009) Physical properties of rice bran wax in bulk and organogels. *J Am Oil Chem Soc* 86:1163–1173. doi:10.1007/s11746-009-1464-6
- Briard AJ, Bouroukba M, Petitjean D, Hubert N, Dirand M (2003) Experimental enthalpy increments from the solid phases to the liquid phase of homologous *n*-alkane series (C18 to C38 and C41, C44, C46, C50, C54, and C60). *J Chem Eng Data* 48:497–513. doi:10.1021/je0201368
- Metivaud V, Rajabalee F, Mondieig D, Haget Y, Cuevas-Diarte MA (1999) Solid-solid and solid-liquid equilibria in the heneicosane-docosane binary system. *Chem Mater* 11:117–122. doi:10.1021/cm980737b
- Roblès L, Mondieig D, Haget Y, Cuevas-Diarte MA (1998) Mise au point sur le comportement énergétique et cristallographique des *n*-alcanes. II. Série de C22H46 à C27H56. *J Chim Phys Phys-Chim Biol* 95:92–111. doi:10.1051/jcp:1998111
- Nyburg SC, Potworowski JA (1973) Prediction of unit cells and atomic coordinates for normal alkanes. *Acta Crystallogr B* 29:347–352. doi:10.1107/s0567740873002451
- Garti N, Wellner E, Sarig S (1980) Stearic-acid polymorphs in correlation with crystallization conditions and solvents. *Krist Tech* 15(11):1303–1310. doi:10.1002/crat.19800151112
- Chevallier V, Bouroukba M, Petitjean D, Barth D, Dupuis P, Dirand M (2001) Temperatures and enthalpies of solid-solid and melting transitions of the odd-numbered *n*-alkanes C21, C23, C25, C27, and C29. *J Chem Eng Data* 46(5):1114–1122. doi:10.1021/je0003501
- Timms RE (2003) *Confectionery fats handbook*. Oily Press, Bridgewater
- Craven RJ, Lencki RW (2011) Binary phase behavior of diacid 1,3-diacylglycerols. *J Am Oil Chem Soc* 88(8):1125–1134. doi:10.1007/s11746-011-1777-0
- Granasy L et al (2005) Growth and form of spherulites. *Phys Rev E* 72(1):011605-1–011605-15. doi:10.1103/PhysRevE.72.011605
- Viswanath D, Ghosh T, Prasad DL, Dutt NK, Rani K (2007) *Viscosity of liquids: theory estimation and data*. Springer, Dordrecht